agriculture

MDPI

Article

Using UAV Images and Phenotypic Traits to Predict Potato Morphology and Yield in Peru

Dennis Ccopi [1], Kevin Ortega [1,*], Italo Castañeda [1], Claudia Rios [1,2], Lucia Enriquez [1], Solanch Patricio [1,2], Zoila Ore [3], David Casanova [3], Alex Agurto [3], Noemi Zuñiga [2,4] and Julio Urquizo [1,2]

[1] Dirección de Desarrollo Tecnológico Agrario, Instituto Nacional de Innovación Agraria (INIA), Carretera Saños Grande, Hualahoyo Km 8 Santa Ana, Huancayo 12007, Peru; dennisccopit@gmail.com (D.C.); mict11000@gmail.com (I.C.); claudiario090@gmail.com (C.R.); luciacep7@gmail.com (L.E.); solanch.patricio.r@gmail.com (S.P.); juliocesarub3@gmail.com (J.U.)
[2] Facultad de Agronomía, Universidad Nacional de Centro del Perú, Carretera Central Km 37, El Mantaro, Jauja 12150, Peru; lzuniga@inia.gob.pe
[3] Dirección de Desarrollo Tecnológico Agrario, Instituto Nacional de Innovación Agraria (INIA), Av. La Molina, 1981, Lima 15024, Peru; zoilaoreaq@gmail.com (Z.O.); dcasanova@inia.gob.pe (D.C.); coordinadoragpres@inia.gob.pe (A.A.)
[4] Programa Nacional de Raíces y Tuberosas, Estación Experimental Agraria Santa Ana, Instituto Nacional de Innovación Agraria (INIA), Carretera Saños Grande, Hualahoyo Km 8 Santa Ana, Huancayo 12007, Peru
* Correspondence: kevinorqu@gmail.com; Tel.: +51-992656272

Abstract: Precision agriculture aims to improve crop management using advanced analytical tools. In this context, the objective of this study is to develop an innovative predictive model to estimate the yield and morphological quality, such as the circularity and length–width ratio of potato tubers, based on phenotypic characteristics of plants and data captured through spectral cameras equipped on UAVs. For this purpose, the experiment was carried out at the Santa Ana Experimental Station in the central Peruvian Andes, where advanced potato clones were planted in December 2023 under three levels of fertilization. Random Forest, XGBoost, and Support Vector Machine models were used to predict yield and quality parameters, such as circularity and the length–width ratio. The results showed that Random Forest and XGBoost achieved high accuracy in yield prediction ($R^2 > 0.74$). In contrast, the prediction of morphological quality was less accurate, with Random Forest standing out as the most reliable model ($R^2 = 0.55$ for circularity). Spectral data significantly improved the predictive capacity compared to agronomic data alone. We conclude that integrating spectral indices and multitemporal data into predictive models improved the accuracy in estimating yield and certain morphological traits, offering key opportunities to optimize agricultural management.

Keywords: crop monitoring; machine learning; precision agriculture; remote sensing; agricultural innovation

Citation: Ccopi, D.; Ortega, K.; Castañeda, I.; Rios, C.; Enriquez, L.; Patricio, S.; Ore, Z.; Casanova, D.; Agurto, A.; Zuñiga, N.; et al. Using UAV Images and Phenotypic Traits to Predict Potato Morphology and Yield in Peru. *Agriculture* **2024**, *14*, 1876. https://doi.org/10.3390/agriculture14111876

Academic Editor: Jiyu Li

Received: 23 September 2024
Revised: 21 October 2024
Accepted: 22 October 2024
Published: 24 October 2024

1. Introduction

Agriculture continues to be a crucial development engine for most countries worldwide [1,2]. In this context, potato (*Solanum tuberosum* L.) stands out as a highly diverse crop in terms of physicochemical characteristics, ranking fourth globally in production and establishing itself as one of the most important and representative crops in the world [3,4]. This tuber is widely consumed in Europe, the United States, and Latin America, where it forms an essential part of the diet and agricultural economy [2,5]. Likewise, potato production is fundamental in the central Andean region of Peru, where various varieties adapted to local microclimates are cultivated [6]. We know its importance, but in the face of accelerated population growth, food scarcity, and climate change, it is urgent to improve the yield and quality of this crop, as well as reduce post-harvest losses. Moreover, with the population projected to reach 9.7 billion by 2050, increasing agricultural production will be essential to meet the growing demand for food [7]. Therefore, it is crucial to promote

its development to offer not only better yield and quality but also greater resistance to environmental, biotic, and abiotic stressors [8–10]. These characteristics are represented through its phenotyping [11].

Obtaining crop phenotypic traits encompasses methodologies and protocols to accurately measure plant growth, architecture, and composition at different scales [12], being fundamental for selecting optimal phenotypes through precise measurement of crop traits. Phenotyping continues to be a challenge in plant breeding, as current techniques for accurately recording important agronomic traits and monitoring crops have not advanced sufficiently [13]. The traditional phenotyping method has been a significant limitation in recent decades due to its high labor demand, the prolonged time it requires, and its low efficiency [14].

However, recent technological advances offer promising solutions to overcome these challenges, allowing the exploration of advanced methods for large-scale phenotypic data acquisition and processing [8,15]. Image-based phenotyping has the potential to dramatically improve our ability to characterize crop phenotypes [13]. These variables, such as compound leaf area (CLA), leaf area (LA), plant height (H), number of stems (S), and the Soil Plant Analysis Development (SPAD) index, are fundamental for understanding crop health and productivity [16]. UAV-based plant phenotyping allows the analysis of various phenotypes with greater precision and efficiency, without the need for intensive human labor, facilitating the study of gene expression in response to current and future agricultural challenges [17–19].

The integration of multitemporal phenotypic data and aerial images to predict crop yield and quality parameters is a rapidly growing field within precision agriculture [20]. Recent studies have shown that spectral indices derived from remote sensors are highly effective for monitoring crops, such as wheat [21,22] and rice [23], allowing accurate estimates of agricultural yield [24–26]. Regarding quality parameters, such as circularity and the length–width ratio, these are essential for accurate phenotyping of external crop attributes, which is crucial for their improvement. Currently, the evaluation of tuber shape, especially in potato crops [27,28], along with density, is based on subjective visual assessment. However, this type of manual evaluation hinders reliable phenotyping of these and other important geometric traits, such as shape uniformity [29]. Therefore, the integration of phenotypic data, such as leaf area, height, and quality parameters, along with aerial images, provides a more comprehensive view of the crop status, improving the accuracy of predictions [30–32].

Furthermore, the use of deep learning techniques and growth models integrated with remote data has increased the precision of these predictions [33–35]. This conglomerate of methodologies has been applied to various crops, demonstrating its versatility [36–38]. Similarly, the integration of crop coefficient data and coverages captured with UAVs, such as NDVI, has also improved estimates in crops, such as sugarcane [39,40], corn [41], and other crops.

In the last decade, UAVs have become a key tool for collecting high-spatial-resolution data in real time [42]. Although they have been widely used in plant phenotyping and crop improvement, few studies have explored their use for mapping phenotypic traits of potatoes. Sankaran et al. [43] analyzed the correlation between characteristics captured from multispectral and thermal UAV images and variables, such as stomatal conductance, plant height, and yield, under different irrigation conditions. Ivushkin et al. [44], for their part, demonstrated that the combination of LiDAR, thermal camera, and multispectral data mounted on UAVs improved the prediction of stomatal conductance using a multiple linear regression model.

However, apart from these studies, there is not much research using UAVs to predict phenotypic traits of potatoes. The integration of emerging technologies, such as unmanned aerial vehicles (UAVs), offers an advanced solution to overcome these limitations. UAVs equipped with multispectral sensors provide high spectral, spatial, and temporal resolution data that can be correlated with variables such as plant height and other phenotypic

characteristics [45]. These data allow for rapid and non-destructive assessment of crop status, thus optimizing resource use and improving production [46].

Based on this approach, this study aims to develop an innovative predictive model to estimate the yield and morphological quality, such as circularity and the length–width ratio, of potato tubers based on phenotypic characteristics of plants and data captured through spectral cameras equipped on UAVs. This direction will not only allow optimization of cultivation practices and maximize both tuber yield and quality but will also contribute to the UN's Sustainable Development Goals (SDGs), specifically SDG 2: Zero Hunger, by increasing agricultural productivity and improving food security, and SDG 13: Climate Action, by promoting resilient agricultural practices that increase adaptability to climate change [47,48].

2. Materials and Methods

2.1. Study Site

The study was conducted in the central region of Peru, at the Santa Ana Experimental Station of the Instituto Nacional de Innovación Agraria (INIA), located in the district of El Tambo, province of Huancayo, department of Junín in Peru (Figure 1). The geodesic coordinates are 75°13′17.60″ W and 12°0′42.36″ S, with an altitude ranging between 3303 and 3325 m above sea level. The region's climate has a rainy season from November to March, a transition phase between April and October, and a dry season from May to August, accumulating a total annual precipitation of 477 mm. Average temperatures range between 3.90 and 20.2 °C, with the lowest temperatures and frequent frosts recorded during the months of May to August [49–51].

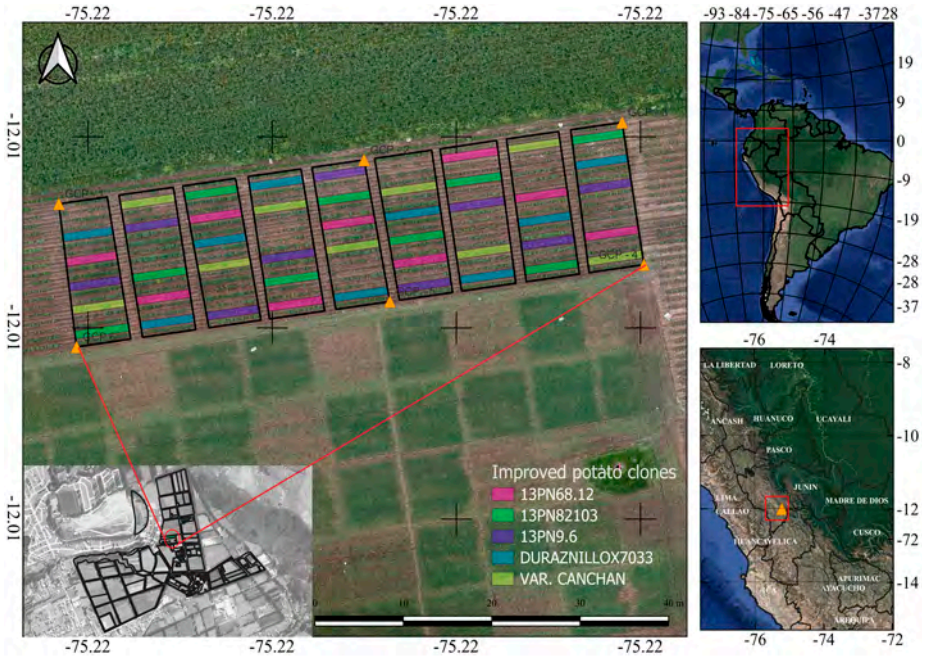

Figure 1. Location of the experimental plot in this study.

The experiment's harvest was conducted on 11 June 2024. In this study, four advanced potato clones were planted along with the Canchan cultivar on 16 December 2023. The clones were obtained from crosses between selected parents, specifically the native potato "Muru Vaccapa Ccallun" and "RC 1445.43B". The evaluated clones were CL1 (13PN83.103), CL2 (Duraznillo 703352.1), CL3 (13PN4.6), and CL5 (13PN68.12). The Canchan cultivar was used as a reference in this study, as its phenotypic characteristics are known. These clones, developed by INIA, are distinguished by their agronomic characteristics and productive potential.

2.2. Experimental Design

For the study, a Randomized Complete Block (RCB) experimental design was used with three fertilization levels. The 'Low' fertilization treatment did not include added amounts of nitrogen (N), phosphorus (P), or potassium (K). For the 'Medium' level, the formula N (160), P (180), and K (160), in kg/ha, was applied, while for the 'High' level, the formula N (180), P (240), and K (180) kg/ha was used. These treatments were applied to the crop plots, as represented in Figure 2. The terrain was subdivided into 9 homogeneous blocks, each with 6 sampling rows. The treatments were assigned so that each potato clone would be replicated in each block, maintaining uniform growth conditions and controlling unwanted variability.

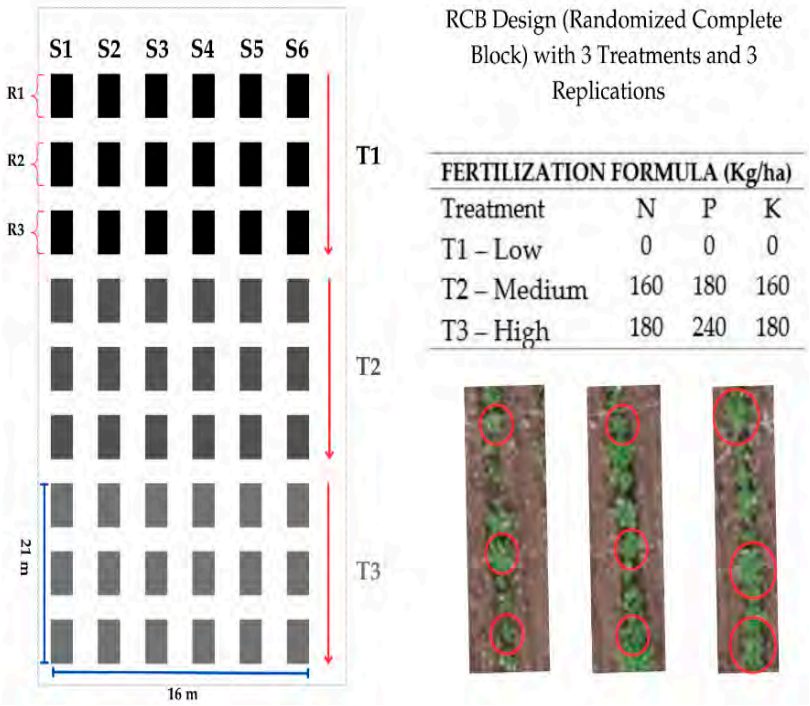

Figure 2. Experimental design with 6 sampling rows (S) and 3 treatments (T), each with 3 replications (R), developing a Randomized Complete Block (RCB) design.

Each experimental plot had dimensions of 7 m wide by 21 m long, with 20 potato plants per row. Five plants from each row were selected as samples, choosing them representatively. For this, visible colored ropes were used to mark lines from the center of the plot, measuring 2.5 m toward the edges to identify the plants. Additionally, control points were established with colored tags to recognize each sampled plant, as shown in Figure 2. This design ensured an accurate evaluation of the effect of different fertilization levels on the crops, ensuring a randomized and controlled approach.

2.3. Methodological Framework

Figure 3 presents the comprehensive methodological approach of the study, offering an overview of the sequential and integrated processes. The study was structured in several main phases. The first focused on collecting phenotypic data from the crops, while the second was focused on obtaining information through UAV flights with incorporated multispectral cameras. The third phase was dedicated to taking photographs of the tubers to extract phenotypic metrics. The fourth phase encompassed the extraction of spectral indices and photogrammetric processes and, finally, integrating all the previous processes, the training and validation of predictive models were carried out.

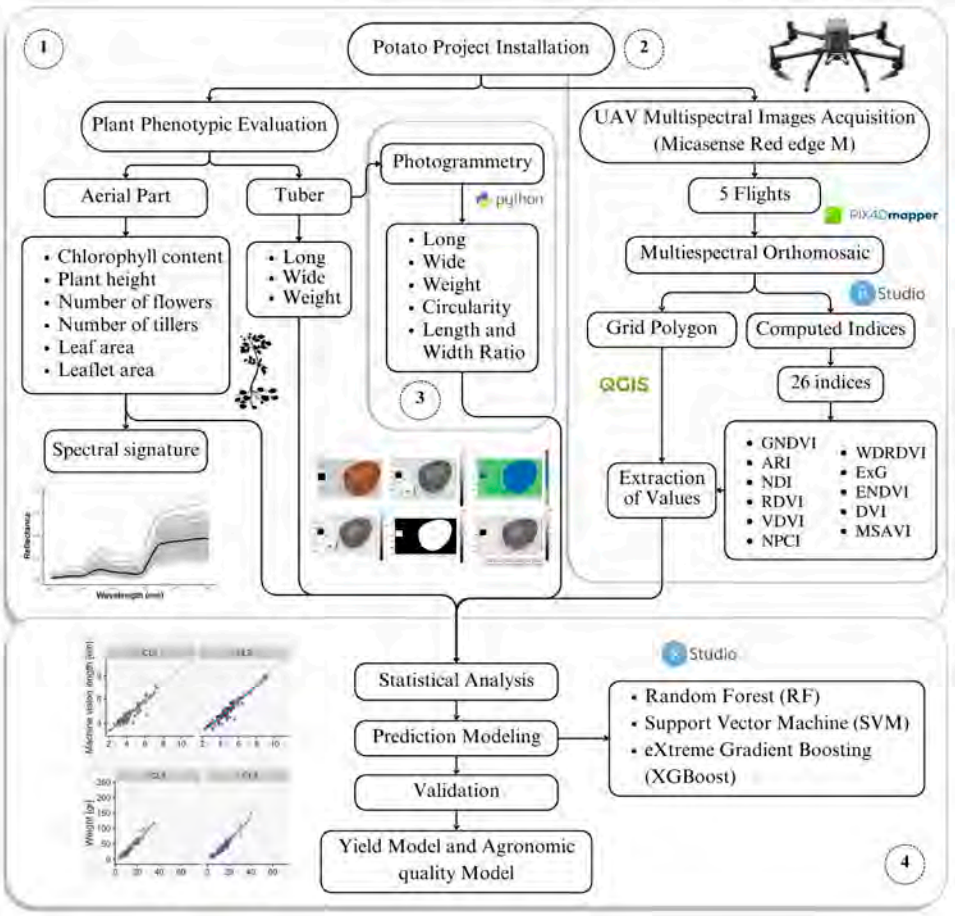

Figure 3. The global methodological approach of the study.

2.4. Image Acquisition and Preprocessing

The experiment was conducted with a MicaSense Red Edge M multispectral camera (Seattle, WA, USA) mounted on a DJI Matrice 300 RTK drone (DJI Technology Co., Ltd., Shenzhen, China). This camera captures 16-bit digital multispectral images in 5 spectral bands: blue (475 ± 32 nm), green (560 ± 27 nm), red (668 ± 14 nm), near-infrared (NIR, 842 ± 40 nm), and red edge (RE, 717 ± 12 nm), with a resolution of 1.6 megapixels (1456 × 1088 pixels). To improve the geospatial accuracy, a GNSS receiver (DJI D-RTK2 Mobile Station, China) was used as a real-time kinematic (RTK) base station. Figure 4 shows the equipment used for capturing multispectral images in the field evaluation.

The flight was executed around noon at a height of 40 m, capturing images every 2 s, with a 75% front and side overlap in 16-bit .tiff format. Eight ground control points were used to geolocate the images and correct possible deviations. Subsequently, the images were integrated into a continuous mosaic, correcting distortions and perspective differences. The MicaSense Red Edge M camera performed an average of 5 flights during key phenological stages of the crop, with an approximate flight time of 3 min and 45 s per flight. Radiometric calibration was performed to adjust variations in lighting and atmospheric conditions, and photogrammetric processing with the Pix4D Pro Mapper produced a high-resolution orthomosaic with a Ground Sample Distance (GSD) of 2.8 cm. Finally, spectral index maps were generated, such as the NDVI (Normalized Difference Vegetation Index), among others, to analyze the crop status, which would be the necessary inputs for subsequent modeling.

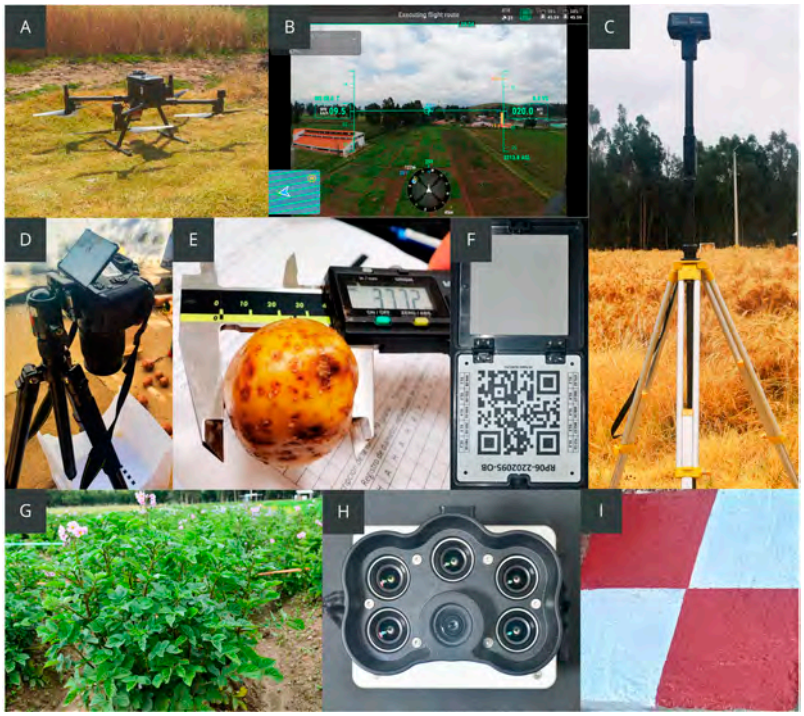

Figure 4. (**A**) UAV Matrice 300, (**B**) flight plan, (**C**) DJI RTK V2 GNSS, (**D**) Nikon D7500 18–140 mm f/3.5–5.6 G photographic camera, (**E**) evaluated potato sample, (**F**) Calibrated Reflectance Panel (CRP), (**G**) crop plot, (**H**) MicaSense Red Edge M camera, and (**I**) ground control point.

2.4.1. Extraction and Processing of Spectral Images of the Plants

For the extraction of indices, derived spectral bands were used based on bibliographic equations from the Terra package [52]. With the calculated indices, a 30 cm buffer was generated around the central point of each plant, and within this area, zonal statistics were applied to extract the maximum values of all pixels contained in the buffer.

To develop the reference models, a set of 11 spectral indices was initially generated, including vegetation and soil indices, all related to crop biomass. For each sampled point, a circular buffer with a radius of 0.25 m was used. Vegetation indices were calculated through different reflectance combinations and compiled as predictors, along with pure spectral bands (Table 1).

Table 1. Spectral indices derived from UAV-acquired multispectral images.

Indices		Expression	Reference
Green Normalized Difference Vegetation Index	GNDVI	$\frac{Nir-Green}{Nir+Green}$	[53]
Renormalized Difference Vegetation Index	RDVI	$\frac{Nir-Red}{\sqrt{Nir+Red}}$	[54]
Visible Difference Vegetation Index	VDVI	$\frac{Nir-Red}{Nir+Red+Green}$	[55]
Wide Dynamic Range Vegetation Index	WDRDVI	$\frac{(Nir-Red)}{\sqrt{Nir+Red}}$	[56]
Modified Soil Adjusted Vegetation Index	MSAVI	$\frac{2\times Nir+1\ \sqrt{(2\ \times\ Nir+1)^2-8\times(Nir-Red)}}{2}$	[57]
Normalized Pigment Chlorophyll Reflectance Index	NPCI	$\frac{Red-Blue}{Red+Blue}$	[58]
Anthocyanin Reflectance Index	ARI	$\frac{1}{Green}-\frac{1}{Red}$	[59,60]
Enhanced Normalized Difference Vegetation Index	ENDVI	$\frac{2\times Nir-Red-Blue}{2\times Nir+Red+Blue}$	[61]
Normalized Difference Index	NDI	$\frac{Green-Red}{Green+Red}$	[60]
Excess Green	ExG	2 − Green − Red − Blue	[60]
Difference Vegetation Index	DVI	NIR − Red	[62]

Note. Multispectral imagery central wavelengths—Blue, Green, Red, and NIR: 474, 560, 668, and 840 nm, respectively.

For multispectral data processing, Pix4D Pro Mapper v4.8.4 software (Prilly, Switzerland) was used, which allowed the creation of detailed orthomosaics from the images captured by the UAV. During this process, digital elevation models were generated, and spectral data were merged to improve image resolution.

The analysis and manipulation of geospatial data were carried out in R Studio v 4.4.1 (R Core Team, Vienna, Austria), using the Terra package [52]. Additionally, Quantum Geographic Information System software (QGIS 2.18.14, QGIS Development Team, Raleigh, NC, USA) was used for image processing and vectorization.

2.4.2. Images of the Tubers

Here, 450 high-quality photographs were captured in JPEG format with a resolution of 300 dpi and dimensions of 4000 × 6000 pixels using a Nikon D7500 DSLR camera with an 18–140 mm lens (Nikon Corporation, Tokyo, Japan). The images were taken in a lightbox with a white background and diffused natural light, and each photograph included a 1 × 1 cm scale. The study included four potato clones and an additional variety, with ten tubers photographed per plant sample. In total, 90 tuber photographs were captured for each clone and variety. The images were cropped to delimit the area and were used to extract tuber phenotypic variables, such as length, width, area, length–width ratio, and circularity, through Equation (1), established in [63]:

$$\text{Circularity} = \left(\frac{\text{Perimeter}^2}{4\pi} \right) \times \text{Area} \quad (1)$$

The extraction of tuber phenotypic variables was performed using Python v3.10 programming language (Python Software Foundation) in the Spyder v5 development environment (Spyder Project Contributors). In the image analysis, various packages were used to ensure precise and efficient processing: OpenCV [64] for advanced image processing operations, NumPy [65] for handling and manipulating data arrays, and Matplotlib [66] for image visualization and annotation. These packages provided the necessary tools for detailed analysis of the captured images.

First, the images were processed by converting them to grayscale. Then, an average filter with a 21-pixel window was applied to smooth them, using a convolution operation. Subsequently, binarization was carried out based on a threshold determined after inspecting the histogram of intensity values. This procedure facilitated segmentation and allowed clear identification of the present elements, such as the scale, the tuber, and the background. To determine the scale and calculate the pixel size in centimeters, Equation (2), referenced in [67], was used:

$$\text{Pixel Size} = \left(\frac{\left(\left(\frac{1}{w} \right) + \left(\frac{1}{h} \right) \right)}{2} \right) \quad (2)$$

Using the scale as a reference, the pixels that make up the tuber were calculated, and the corresponding metrics were extracted. Subsequently, a linear regression analysis was performed with the data measured with the vernier to evaluate the degree of correspondence. These parameters are fundamental for evaluating tuber quality according to their intended use, whether for industrial or food applications [67,68].

2.5. Field Data Acquisition

The collection of phenotypic traits in potato plants was carried out at three different times during crop development, selecting crucial phenological stages for data collection: tuber initiation, flowering, and maturity. These stages were established at 59, 79, and 95 days after planting, respectively [69,70].

At each of these stages, phenotypic data, such as leaf area, compound leaf area, stem count, chlorophyll index, and plant height, were recorded. Additionally, supplementary

data were collected, including stem, flower, and leaf color, flower count, and the number of berries formed by each evaluated plant.

For phenotypic data collection, flexometers were used to measure the height and radii of leaf area and compound leaves, following the methodology proposed in [71] and expressed in Equation (3). To measure the chlorophyll index, SPAD 502 PLUS equipment (Minolta Camera Co., Ltd., Tokyo, Japan) was used.

$$AL = \pi \times \left(\frac{a}{2}\right) \times \left(\frac{b}{2}\right) = \pi\left(\frac{a \times b}{4}\right) \quad (3)$$

2.6. Data Analysis and Selection of Predictor Variables

For data analysis and predictor variable selection, several detailed procedures were carried out. Initially, flights were conducted with the DJI Matrice 300 RTK UAV (DJI Technology Co., Ltd., Shenzhen, China) at different intervals after planting: at 76, 82, 86, 108, and 128 days. Once the images were captured and obtained, they were aligned and corrected using georeferenced control points established on the ground to ensure precision in geolocation.

Subsequently, 11 spectral indices were extracted from each set of images, along with the original spectral bands. These indices and bands were combined to construct a correlation matrix that integrated field variables, organized in columns corresponding to days 59, 79, and 95, taking into account each variable and spectral index. This matrix was key to identifying the variables most related to the metrics of interest. Subsequently, a principal component analysis (PCA) was carried out. This approach allowed for reducing the dimensionality [72] of the data and identifying variables that significantly contributed to data variability. The PCA facilitated the selection of optimal variables for predictive models, allowing for a more precise evaluation of predictor variables that influence crop quality and yield.

2.7. Modeling and Prediction Algorithms

Among the chosen prediction algorithms, Support Vector Machine (SVM) is a machine learning algorithm widely used in precision agriculture for crop prediction and management. SVM stands out for its ability to analyze and classify complex data by creating an optimal hyperplane that separates different classes in the dataset. In agriculture, SVM is used to predict crop yields, identify diseases, and classify the quality of agricultural products. Its ability to handle large volumes of data with multiple variables makes it a crucial tool for optimizing production and managing resources efficiently [73–75].

Random Forest (RF) is a machine learning model widely used in agriculture to forecast yield and manage crops. This model generates several decision trees from random subsets of the original dataset and then combines the predictions of these trees to improve accuracy and reduce the risk of overfitting. The robustness of RF makes it particularly effective in addressing the variability of agricultural data and providing reliable predictions on crop yield, soil conditions, and pest or disease detection [76,77].

Extreme Gradient Boosting (XGBoost) is used in the agricultural field due to its ability to handle large volumes of heterogeneous data, such as phenotypic, meteorological, and aerial image measurements, improving the accuracy of predictions in crops, such as wheat, rice, and potatoes. Its main virtues include efficient data handling, its ability to identify the importance of key variables, treatment of missing values, and prevention of overfitting thanks to regularization. This allows for generating robust and precise predictions, optimizing agricultural management, and facilitating informed decision-making regarding crop yield and management [78–80].

2.8. Optimization and Evaluation of Models

In the process of optimizing and training the Random Forest, SVM, and XGBoost models, K-fold cross-validation was applied to evaluate performance and select the best hyperparameters [81–83]. In this approach, the dataset was divided into k subsets or "folds" of equal size; in this study, 10 of these sets were used. For each set of hyperparameters tested, the model was trained on $K - 1$ of these subsets and validated on the remaining fold. This procedure was repeated K times, ensuring that each fold was used as a validation set exactly once.

This cross-validation method not only helps adjust hyperparameters to obtain the best performance but also ensures that the model is robust and generalizes well to unseen data. By averaging the performance metrics (R^2, RMSE, and MAE) obtained in each fold, an optimal estimate of performance in the test dataset was obtained. Thus, the trained model was evaluated on multiple subsets of the dataset, reducing bias and variance in the evaluation of its performance.

2.9. Model Evaluation Metrics

The metrics R^2 (coefficient of determination), RMSE (root mean square error), and MAE (mean absolute error) were employed to evaluate the accuracy and performance of the prediction models [84]. R^2 indicates how well the model captures the variability of the observed data by measuring the proportion of variance in the dependent variable explained by the independent variables.

An R^2 value close to 1 indicates a strong fit, while values close to 0 suggest that the model does not adequately explain the data [85,86]. RMSE reflects the average magnitude of errors in predictions, placing a greater penalty on larger errors by squaring the differences between observed and predicted values, making it a useful metric when large errors are especially undesirable.

On the other hand, MAE provides a direct measure of average error and is less sensitive to extreme errors than RMSE, making it suitable when a robust metric against outliers is sought [87,88]. These metrics provide a comprehensive view of model performance, aiding in the selection of the best model based on the context and nature of the data.

3. Results

3.1. Descriptive Statistics of Agronomic Variables

Table 2 shows the descriptive analysis of phenotypic traits related to crop growth taken in the field, as well as the morphological quality parameters of the potato determined from the photometric process.

Table 2. Descriptive statistics of agronomic variables.

Agronomic Variable	Prom.	Mean	Min.	Max.	σ
Height (meters) (H)	0.29	0.28	0.02	0.70	0.13
Tillers (T)	3.09	3.00	1.00	22.00	1.30
Leaflet area (square meters) (CLA)	0.01	0.01	0.00	0.16	0.01
Leaf area (square meters) (LA)	0.11	0.09	0.00	0.55	0.08
SPAD	42.80	43.30	20.60	66.20	7.08
Tuber weight (kilograms) (WP)	0.04	0.04	0.01	0.20	0.03
Tubercle area (square meters) (A)	15.90	14.50	1.70	53.30	8.14
Axismajor (centimeter) (MA)	4.86	4.60	1.20	9.60	1.45
Minoraxis (centimeter) (mA)	3.93	3.90	0.90	6.90	0.93
Length and width (LW)	1.08	1.00	0.40	1.80	0.25
Circularity (CIR)	1.21	1.18	0.58	2.95	0.17
Total tuber weight (kilograms) (W)	0.59	0.52	0.12	1.40	0.30

Note: Standard deviation (σ).

The average plant height was 0.29 m, with slight variability (σ = 0.13), while the number of stems showed greater dispersion, with an average of 3.09 and a standard deviation of 1.30. The average leaf area was 0.11 m^2 (σ = 0.08), and the SPAD index, which measures chlorophyll, had an average value of 42.80 (σ = 7.08). The average weight of the tubers was 0.04 kg (σ = 0.03), and their area and dimensions (major and minor axes) showed considerable variability. The total weight of the tubers was 0.59 kg, with a high standard deviation (σ = 0.30), reflecting a great diversity in the size and weight of the analyzed tubers. In general, some variables showed greater consistency, while others, such as the area and weight of the tubers, showed high dispersion.

3.2. Analysis of Treatments

Figure 5 compares the three treatments applied to potato crops (T1, T2, and T3) using box plots that illustrate the height and leaf area. Treatment T2 presented the highest median in height, while T3 stood out in leaf area, with the highest median in this variable. Although T2 excelled in height, T3 showed competitive performance in both metrics, suggesting that it could be the most balanced and effective treatment for optimizing potato crop development.

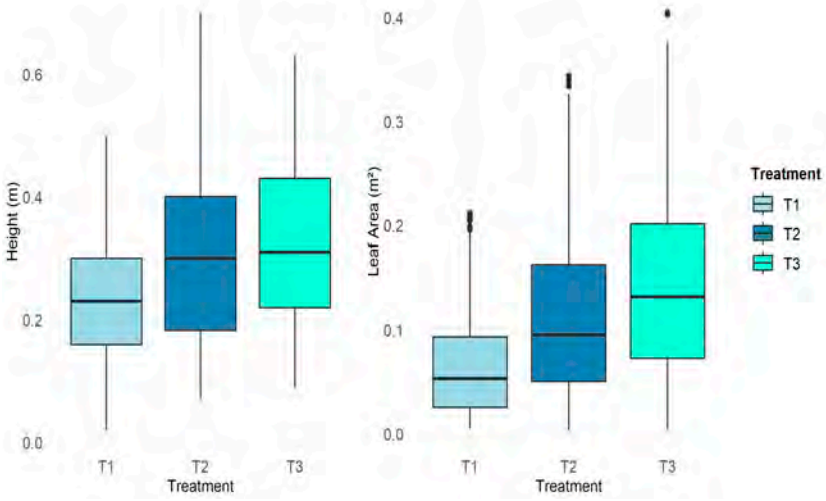

Figure 5. Comparison of the height and leaf area of potato plants under three treatments (T1, T2, and T3).

3.3. Spectral Signatures

Figure 6 shows the spectral reflectance curves of different potato clones across a range of wavelengths, spanning from 400 to 900 nanometers (nm). Each line in the graph represents the reflectance of a specific clone: (CL1) 13PNTN83103 (gray), (CL2) 703352.1 (purple), (CL3) 13PN4.6 (blue), (CL5) 13PN68.12 (orange), and CANCHAN (green). These images were obtained using a Spectral Evolution PSR + 3500 spectroradiometer ('PSR', Spectral Evolution) at 15 cm from the lens for each evaluation.

Each potato clone responded differently to radiation at different wavelengths, which may be related to the composition and structure of their leaves, such as chlorophyll content and other pigments. A significant increase in reflectance was observed within the range of 700 to 900 nm, which is characteristic of the phenomenon known as "Red Edge". This particularity is typical in vegetation and reflects the transition between the visible and near-infrared regions of the spectrum, often associated with plant phenology, health, and vigor [73,89,90]. In particular, the curve corresponding to clone 13PNTN83103 presented the highest reflectance throughout the entire range, which could indicate a greater light absorption capacity or structural differences compared to other clones.

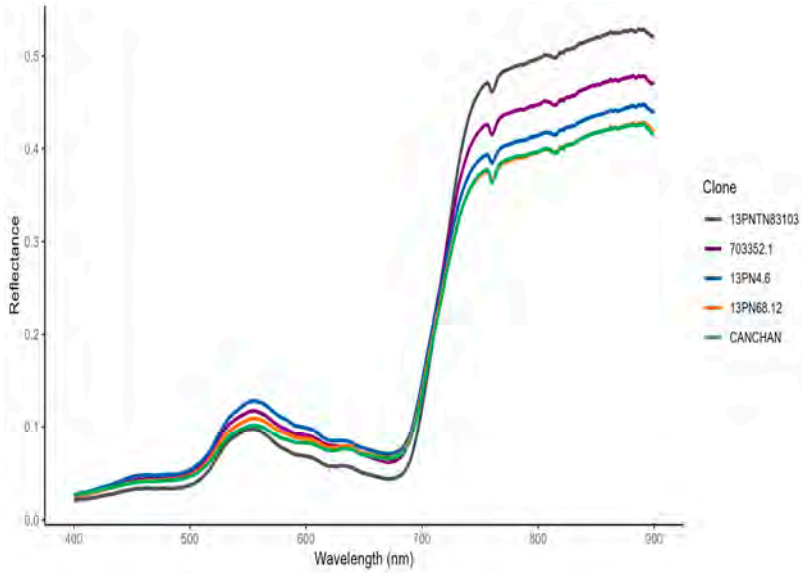

Figure 6. Spectral signatures of potato clones and the Canchan cultivar.

3.4. Analysis of Spectral Variables

Comparison of Photographic Metrics with Field Data

Figure 7 presents four scatter plots that reveal a strong correlation between photographic and manual measurements of potato phenotypic variables. In the upper graphs, the comparison of the minor and major axes, measured manually and from photographs, shows coefficients of determination (R^2) of 0.76 and 0.88, respectively, indicating a positive and significant relationship. These results suggest that photographic measurements are a reliable tool for estimating these dimensions.

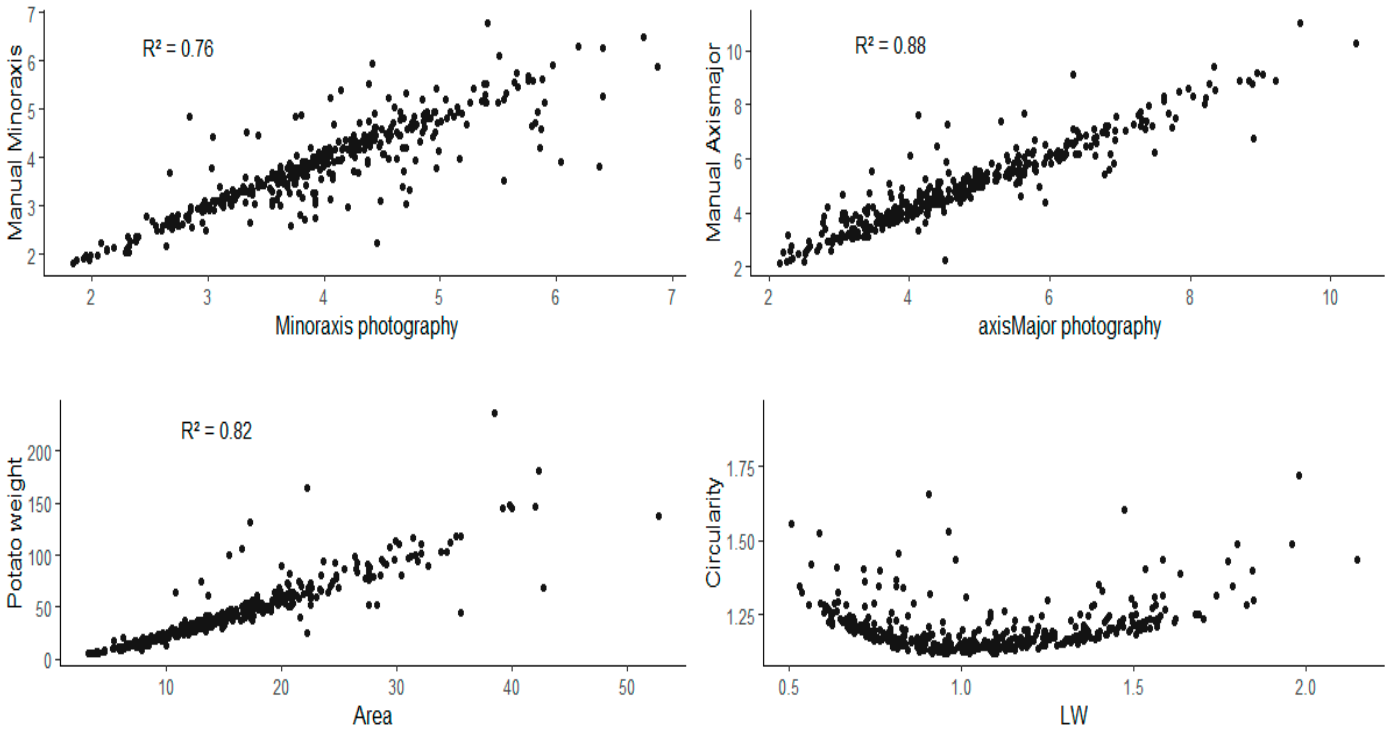

Figure 7. Scatter plots for the comparison of photographic and manual measurements.

In the lower graphs, the area measured from photographs shows a strong correlation (R^2 = 0.82) with potato weight, suggesting that area is a good predictor of this parameter.

However, the relationship between circularity and the length/width ratio of potatoes did not show a linear trend, indicating a possible non-linear relationship and suggesting that other factors could influence tuber shape. This analysis confirms the effectiveness of photographic measurements in automated phenotyping, as the data captured through photometric analyses were used to predict tuber yield and quality.

3.5. Correlation Analysis

Figure 8 shows the Pearson correlation matrix [72] for phenotypic and spectral variables related to tuber growth and characteristics. The morphological quality variable, circularity (CIR), showed low or no correlations with most variables, suggesting that tuber shape did not significantly depend on the evaluated growth characteristics. However, CIR showed moderate negative correlations with the indices NDI_86 (−0.50) and NPCI_86 (−0.40), indicating a possible influence of these indices on the circular shape of the tubers. Similarly, the length and width (LW) variable, which was also related to tuber shape, showed negative correlations with the same indices, suggesting that variations in shape were partially associated with these spectral indicators.

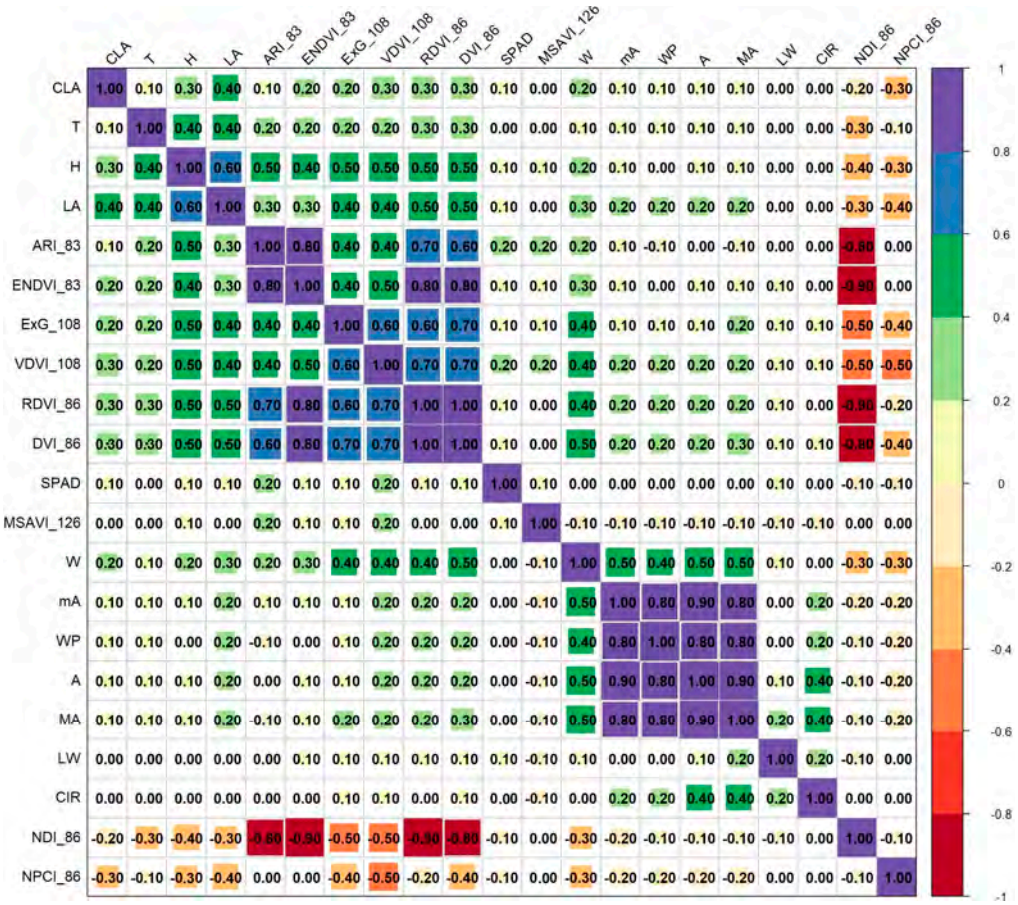

Figure 8. Correlation matrix between phenotypic and spectral variables.

On the other hand, the yield variable, total tuber weight (W), showed stronger positive correlations with various variables, notably, leaf area (LA, 0.70), plant height (H, 0.50), and the spectral indices RDVI_86 (0.70) and VDV_108 (0.50). These correlations suggest that both vegetative growth characteristics and some vegetation indices related to infrared reflectance are good predictors of tuber yield. Furthermore, these results indicate that while agronomic quality (tuber shape) seemed to be less influenced by the measured variables, yield (tuber weight) was strongly associated with vegetative vigor and certain spectral indices.

3.6. Model Performance

3.6.1. Yield Estimation

Figure 9 shows the comparison of estimated potato crop yield using three prediction models: Random Forest (RF), Support Vector Machine (SVM), and XGBoost. In the training set, the RF model achieved high accuracy, with an R^2 value of 0.82 and an RMSE of 0.14, indicating a good fit. However, in the test set, its performance slightly decreased, with an R^2 value of 0.74, suggesting that the model remained reliable for predicting potato crop yield. The SVM model, on the other hand, had moderate accuracy in training (R^2 value of 0.72) but experienced a considerable drop in the test set, with an R^2 value of 0.56, indicating that it might not be as suitable for generalizing yield prediction in potato crops.

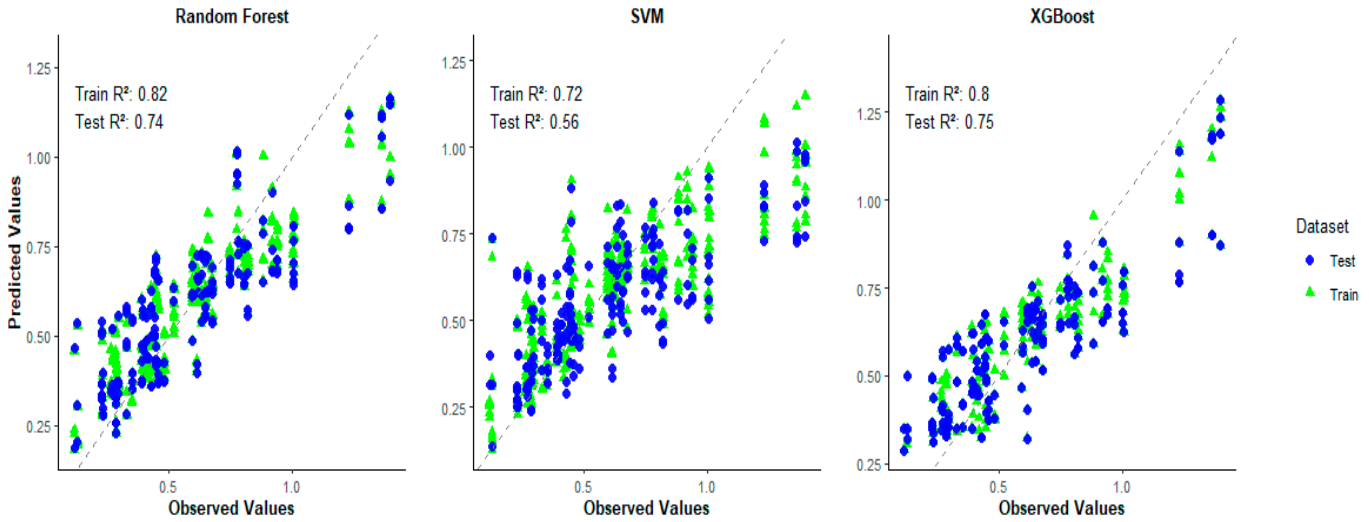

Figure 9. Comparison of estimated potato crop yield using Random Forest, Support Vector Machine (SVM), and XGBoost prediction models.

The XGBoost model offered a more robust balance, presenting a good fit in both training (R^2 value of 0.80) and the test set, where it achieved an R^2 value of 0.75 and an RMSE of 0.17, making it the most effective model of the three for estimating potato crop yield. These results suggest that while all models were useful, XGBoost performed better at accurately predicting yield in new samples, making it more suitable for prediction applications in precision agriculture.

3.6.2. Circularity Estimation

The evaluation of potato circularity prediction was performed using two distinct datasets: the first included agronomic data and spectral indices, while the second was based solely on phenotypic traits. The models were evaluated with data from 79 and 95 days, closer to harvest. Circularity, a crucial indicator of tuber morphological quality, for the first dataset showed that the Random Forest model was the most effective. With an R^2 value of 0.76 in the training set and 0.55 in the test set, Random Forest demonstrated a solid ability to fit the data and generalize to new sets, suggesting a moderate capacity to predict potato circularity accurately (Figure 10a).

In contrast, SVM and XGBoost showed inferior performances. SVM showed a low R^2 value of 0.44 in training and 0.38 in testing, indicating significant difficulties in prediction. XGBoost, despite having an R^2 value of 0.63 in training, suffered from overfitting, with an R^2 value of only 0.06 in the test set. This limited its effectiveness in predicting potato circularity, highlighting RF as the most reliable option for evaluating the morphological quality of tubers.

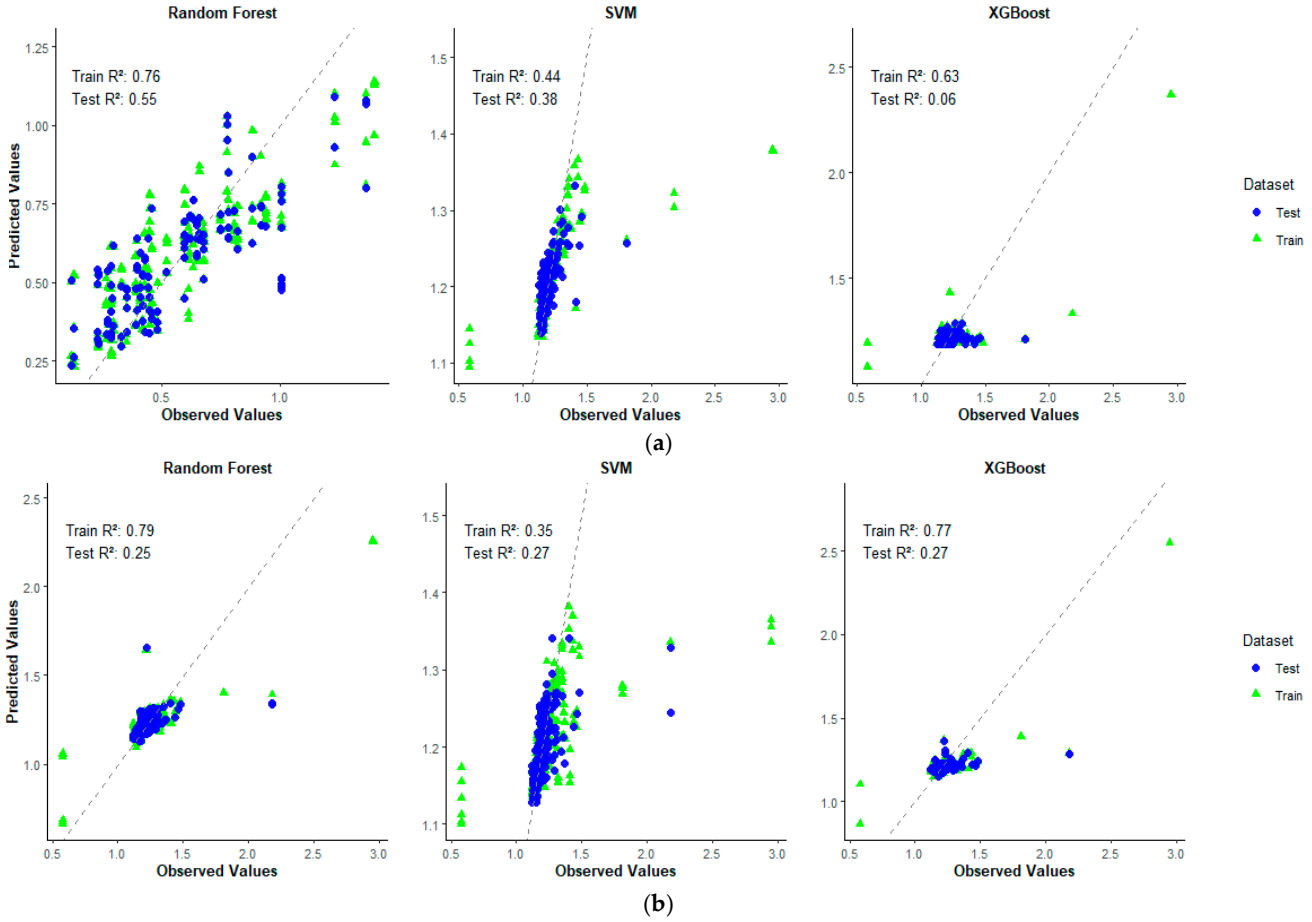

Figure 10. Comparison of estimated potato crop yield: (**a**) using Random Forest (RF), Support Vector Machine (SVM), and XGBoost prediction models, including phenotypic traits and spectral indices, and (**b**) using only phenotypic traits.

For the second dataset, potato circularity estimation was performed using only phenotypic traits. Figure 10b shows the results of the models in terms of predictive accuracy, both in the training and test sets. The RF model presented a high R^2 value in the training set (0.79) but suffered a significant drop in the test set (0.25), suggesting possible overfitting. In contrast, XGBoost showed greater stability between both sets, with an R^2 value of 0.77 in training and 0.27 in testing. The SVM model had a lower performance, with an R^2 value of 0.35 in the training set and 0.27 in the test set. Error metrics, such as RMSE and MAE, were similar among the models, indicating slight differences in their predictive capacity.

3.6.3. Estimation of Plant Length–Width Ratio

The evaluation of the prediction of the potato length and width ratio was performed using two distinct datasets: the first included agronomic data and spectral indices, while the second was based solely on phenotypic traits. The models were evaluated with data from 79 and 95 days, closer to harvest.

Figure 11 shows the comparison of the predictive capacity of Random Forest, Support Vector Machine, and XGBoost models for the length–width ratio of potatoes. In the training set, RF and XGBoost showed a good fit, with R^2 values of 0.78 and 0.75, respectively, while Support Vector Machine reached a value of 0.76. However, all models presented moderate errors (RMSE and MAE), suggesting that, although they fit well with the training data, there was still dispersion in the predictions.

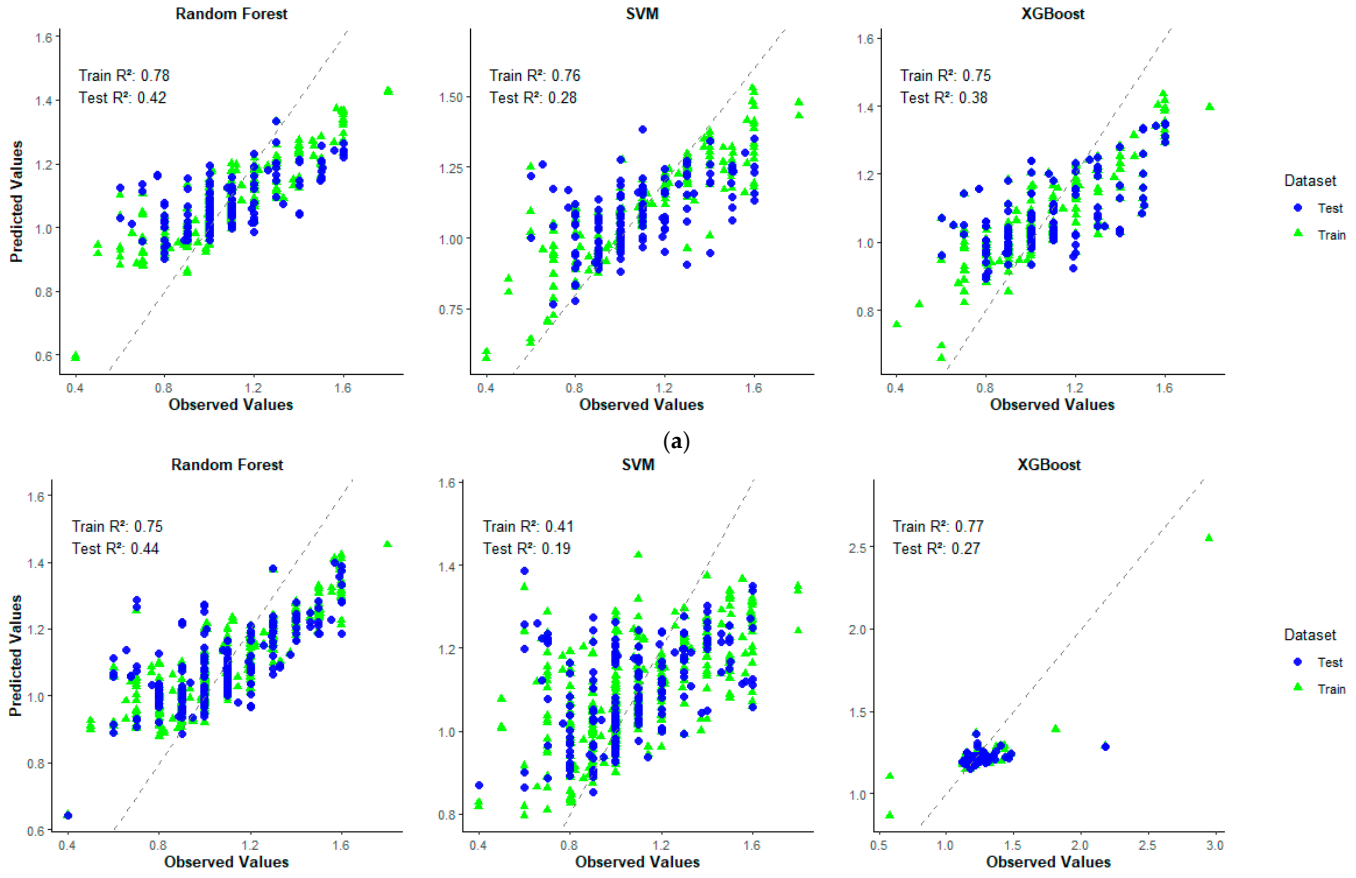

Figure 11. Comparison of the length–width ratios of potato crops: (**a**) using Random Forest, Support Vector Machine (SVM), and XGBoost prediction models, including phenotypic traits and spectral indices, and (**b**) using only phenotypic traits.

In the test set, all three models suffered a decrease in their performance. RF showed a significant drop in its R^2 value to 0.42, while Support Vector Machine and XGBoost decreased to 0.28 and 0.38, respectively. This indicates that the models did not generalize well to new data, possibly due to overfitting. Although Random Forest and XGBoost performed slightly better, all models showed difficulties in correctly predicting the length–width ratio of potatoes in unseen data.

In the second group of data, in training, XGBoost had the best R^2 value, with 0.77, followed by RF with 0.75, both with low errors in RMSE and MAE, indicating a good fit. SVM, on the other hand, showed an R^2 value of 0.41, reflecting difficulties in capturing the length–width ratio of potatoes. In testing, RF reached an R^2 value of 0.44, XGBoost fell to 0.27, and SVM obtained the worst result, with 0.19, suggesting that the models, although effective in training, did not generalize well to new data, indicating possible overfitting, especially in XGBoost.

3.7. Predictor Estimation

Table 3 shows the hyperparameters used for the predictive models used for potato yield and quality prediction (Random Forest, Support Vector Machine, and XGBoost). For the Random Forest model, hyperparameters, such as node size, number of trees, and number of variables per node, were established, with optimal values adjusted for each objective. For example, for weight (W) prediction, 500 trees and a node size of 45 were used, reaching an explained variance value of 65.55%. In contrast, for other objectives, such as CIR, IND, LW, and PT, the hyperparameters were adjusted to find a better response.

Table 3. Characteristics and estimation of predictors.

Models	Targets		Hyperparameters						
RF			Node size	Trees	No. var	Mean of squared	% var		
	W		45	500	6	0.0307	65.55		
	CIR	IND	50	500	6	0.0115	65.51		
		PT	50	500	3	0.0137	59.04		
	LW	IND	50	500	3	0.0375	40.74		
		PT	50	500	3	0.0375	40.74		
MSV			Cost	γ	ε	No. of vectors	SVM		
	W		0.5	0.1	0.1	394	Radial		
	CIR	IND	0.5	0.1	0.1	191	Radial		
		PT	1	0.1	0.1	404	Radial		
	LW	IND	0.5	0.1	0.1	271	Radial		
		PT	1	0.1	0.1	403	Radial		
XGBoost			Nrounds	Max. depth	η	γ	Colsample_bytree	Min_child_weight	Subsample
	W		100	6	0.1	0.5	0.8	1	0.8
	CIR	IND	100	1	0.2	0.5	0.8	1	0.8
		PT	100	6	0.1	0.5	0.8	1	0.8
	LW	IND	100	6	0.2	0.5	0.8	1	0.8
		PT	50	6	0.2	0.5	0.8	1	0.8

Note: CIR = circularity; IND = spectral indices; PT = phenotypic traits; W = total tuber weight; LW = length and width.

As for SVM, parameters such as cost, γ (gamma), ε (epsilon), and the number of support vectors were used, with a radial kernel function for all metrics. The values varied according to the objective, such as a cost of 0.5 and γ of 0.1 for W prediction. Finally, XGBoost was configured with parameters such as the number of rounds (Nrounds), maximum tree depth (max. depth), and learning rate (η), showing specific adjustments for each objective. For example, 100 rounds and a maximum depth of 6 were used for W prediction, achieving optimized accuracy. These adjustments allowed each model to better adapt to the specific characteristics of the input data and improve the prediction accuracy.

Table 4 shows the performance of the predictive models (Random Forest, Support Vector Machine, and XGBoost) in estimating potato weight, circularity, and the length–width ratio. Random Forest offered solid results, with an R^2 value of 0.82 in training and 0.74 in testing for weight prediction, but its performance in circularity with spectral indices CIR and IND decreased in the test data (R^2 = 0.55). Prediction using only agronomic data, CIR and PT, had even lower accuracy in testing (R^2 = 0.25), suggesting that spectral indices are more useful for this task.

Support Vector Machine presented varied performance, with the best results in CIR and IND (R^2 = 0.38 in testing), while CIR and PT had lower performance (R^2 = 0.27). XGBoost also stood out in weight (W) prediction, with an R^2 value of 0.80 in training and 0.75 in testing. However, it had difficulties with circularity, where CIR and IND showed a very low R^2 value in testing (0.06), while CIR and PT had moderate performance (R^2 = 0.27). This indicates that both Random Forest and XGBoost were effective in predicting weight, but faced challenges with circularity, especially when integrating spectral indices.

Table 4. Performance of predictive models in estimating weight, circularity, and the length–width relationship of potatoes.

Models		Targets	Training			Test		
			R^2	RMSE	MAE	R^2	RMSE	MAE
RF	CIR	W	0.82	0.1385	0.1073	0.74	0.1707	0.1327
		IND	0.76	0.1637	0.1282	0.55	0.1887	0.1427
		PT	0.79	0.098	0.0443	0.25	0.1	0.0439
	LW	IND	0.78	0.1557	0.1202	0.42	0.1905	0.1471
		PT	0.75	0.1555	0.1205	0.45	0.1865	0.1441
MSV	CIR	W	0.72	0.1711	0.1098	0.56	0.2171	0.1553
		IND	0.44	0.1617	0.0444	0.38	0.0677	0.0377
		PT	0.35	0.1597	0.0484	0.27	0.1014	0.0408
	LW	IND	0.76	0.1352	0.0828	0.28	0.1996	0.1468
		PT	0.41	0.198	0.1412	0.19	0.2177	0.1588
XGBoost	CIR	W	0.8	0.1491	0.1707	0.75	0.1192	0.1352
		IND	0.63	0.1271	0.0812	0.06	0.0646	0.0503
		PT	0.77	0.0991	0.0566	0.27	0.1053	0.0513
	LW	IND	0.75	0.1159	0.1897	0.38	0.1202	0.1479
		PT	0.7	0.1578	0.1262	0.47	0.1813	0.1421

Note: CIR = circularity; IND = spectral indices; PT = phenotypic traits; W = total tuber weight; LW = length and width.

3.8. Yield Estimation in Plots

Figure 12 shows the prediction map of the final weight of tubers, highlighting the performance of treatments (T1, T2, and T3). The weight was estimated using the Random Forest model, which showed the best performance in predicting both yield and quality. The results are represented by a color scale, ranging from red (0.05–0.2 kg) to dark green and blue (0.9–1.066 kg), indicating the predicted values in kilograms per 0.5 m^2 quadrant. These quadrants were vectorized considering the maximum leaf area (LA) of the potato crop.

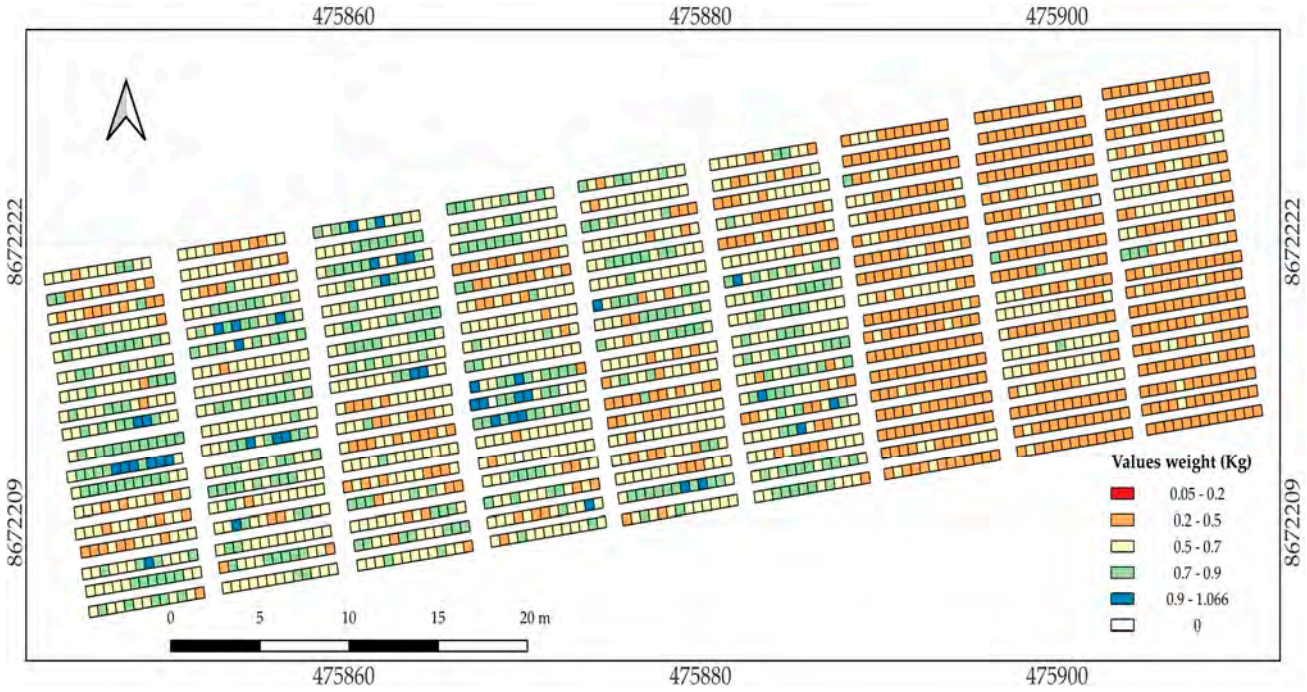

Figure 12. Final tuber weight prediction map.

The descriptive statistics of tuber weight (W), such as median and average, were 0.56 kg and 0.52 kg, respectively. These values reflect the predictive capacity of the Random Forest (RF) model, as they predominated throughout the prediction plot. This behavior further reinforced the performance of the model, which obtained a determination coefficient R^2 value of 0.72 in the testing phase, demonstrating a high prediction capacity. Additionally, the observed minimum and maximum values did not present considerable dispersion concerning the descriptive statistics, which confirmed the accuracy of the model.

4. Discussion

Spectral indices have a variable impact on the predictive capacity of models [60,62,91], especially in morphological quality, such as circularity and the length–width ratio. The prediction of circularity using CIR and IND spectral indices showed a more significant performance, with Random Forest achieving an R^2 value of 0.55 in testing, while XGBoost only achieved 0.06, indicating that these indices moderately captured the variability necessary for this metric. On the other hand, CIR and PT agronomic data were less effective, with an R^2 value of 0.25 in testing for Random Forest and 0.27 for SVM, suggesting that agronomic data alone were not sufficient to accurately predict the various morphological quality parameters of potatoes. These results highlight the need to optimize the integration of spectral indices and agronomic data in predictive models to improve the accuracy of estimating morphological quality.

In the present study, Random Forest and XGBoost showed high accuracy in predicting weight (W), with R^2 values of 0.74 and 0.75 in testing, respectively. Additionally, various studies have highlighted that Random Forest offers a considerable advantage in the optimal selection of variables for yield prediction in different crops [19,92]. Among them, Yiguang et al. [93] proposed an HLM linear model to estimate potato yield using vegetation indices and environmental variables.

The model showed ranges between 0.57 and 0.60 in different growth stages, surpassing conventional methods. This highlighted that vegetation indices in the integration of predictive models and the integration of multitemporal data have shown a significant improvement in the accuracy of yield prediction and the morphological quality of tubers, such as the use of the "substor-potato" model with temporal data of up to nine years, with an R^2 value of 0.97 [94]. Other methods for predicting potato yield, such as the use of physical properties, with the integration of neural networks and other non-linear regression algorithms, have achieved notable results [17].

The accurate estimation of morphological parameters remains a crucial challenge for agriculture, as predicting characteristics such as crop yield and biomass is essential for efficient resource management and optimization of agricultural practices. Despite significant advances in modern techniques, such as remote sensing and machine learning, the transfer and applicability of these models to diverse environmental conditions and growth stages remains limited [95–97]. However, the integration of multitemporal data and the inclusion of specific environmental variables could considerably improve the accuracy of predictions [98–100]. Furthermore, the use of advanced techniques, such as those presented in this study, and the optimal selection of variables offer a key opportunity to overcome these challenges, allowing for more adapted and reliable estimations in different agricultural contexts.

In this study, Random Forest and XGBoost models were used due to their proven effectiveness in predictive tasks and handling high-dimensional data, such as those obtained from multispectral images. While the results showed good performance in predicting potato yield, the accuracy in predicting more complex morphological traits, such as circularity, was relatively low. This limitation may be attributed to the intrinsic nature of morphological traits, which require models capable of capturing more complex, non-linear relationships. Future studies should explore the use of advanced techniques, such as deep learning, which could enhance the predictive capacity for morphological traits, as well as optimizing the current models' hyperparameters. Nonetheless, this work established a solid

foundation from which more sophisticated approaches can be developed, highlighting the potential of integrating multispectral imagery and phenotypic data in precision agriculture.

5. Conclusions

The integration of spectral indices in estimating the physical characteristics of potatoes, such as circularity, significantly influenced the precision and efficiency of morphological evaluation of crops. By incorporating these indices, the ability to characterize key aspects of the tuber was improved, resulting in a more accurate estimation of important parameters for agricultural management and product quality. Advanced techniques, such as the use of hyperspectral images and machine learning models, have proven to be particularly effective in capturing details that traditional methodologies might overlook. These approaches not only optimize the detection of morphological characteristics but also allow for better adaptation to different environmental conditions and growth stages.

The prediction of tuber quality, evaluated through circularity and the length–width ratio, showed the lowest determination coefficients in the XGBoost and SVM models. However, for circularity, the RF model performed better, although it presented significant overfitting. This suggests the need for further research to identify optimal predictive variables that allow accurate prediction of circularity, a key phenotypic trait related to potato quality.

Yield and quality prediction using UAVs face several limitations, including the influence of environmental conditions, such as cloud cover and variations in sunlight, which can affect the quality of captured images. Additionally, the surface information provided by UAVs may not accurately reflect the internal conditions of the crop, limiting the accuracy of estimating key parameters. The selection of predictive variables also presented challenges, with the risk of overfitting or lack of generalization in the models. Moreover, the high demand for computational resources and the need to validate results with field data made it difficult to apply these models on a large scale. This highlights the importance of continuing research to improve both the accuracy and efficiency of predictive models.

Author Contributions: D.C. (Dennis Ccopi), K.O., J.U. and I.C., conceptualization; D.C. (Dennis Ccopi), I.C., D.C. (David Casanova) and A.A., methodology; D.C. (Dennis Ccopi), I.C., Z.O., N.Z. and C.R., software; J.U. and K.O., validation; J.U., L.E., D.C. (David Casanova), K.O. and I.C., formal analysis; C.R. and S.P., investigation; J.U., D.C. (Dennis Ccopi), K.O., I.C. and S.P., resources; I.C., L.E., D.C. (David Casanova) and A.A., data curation; K.O., writing—original draft preparation; K.O. and Z.O., writing—review and editing; D.C. (Dennis Ccopi), Z.O., N.Z. and L.E., visualization; I.C., S.P., D.C. (Dennis Ccopi) and A.A., supervision; C.R., J.U., N.Z., D.C. (David Casanova) and A.A., funding acquisition. All authors have read and agreed to the published version of the manuscript.

Funding: This research was funded by the project "Creación del servicio de agricultura de precisión en los Departamentos de Lambayeque, Huancavelica, Ucayali y San Martín 4 Departamentos" of the Ministry of Agrarian Development and Irrigation (MIDAGRI) of the Peruvian Government, with grant number CUI 2449640.

Institutional Review Board Statement: Not applicable.

Data Availability Statement: The original contributions presented in the study are included in the article. Further inquiries can be directed to the corresponding author.

Acknowledgments: Special thanks are extended to the collaborators involved in field data collection, the assistants of the Precision Agriculture Project (CUI 2449640), and the team members of other research programs at the "Estación Experimental Santa Ana", INIA. I would also like to express my gratitude to Diego Fernández Ibarra for his valuable knowledge and ongoing support.

Conflicts of Interest: The authors declare no conflicts of interest.

References

1. Amoros, W.; Salas, E.; Hualla, V.; Burgos, G.; De Boeck, B.; Eyzaguirre, R.; Felde, T.; Bonierbale, M. Heritability and genetic gains for iron and zinc concentration in diploid potato. *Crop Sci.* **2020**, *60*, 1884–1896. [CrossRef]
2. Devaux, A.; Goffart, J.P.; Kromann, P.; Andrade-Piedra, J.; Polar, V.; Hareau, G. The Potato of the Future: Opportunities and Challenges in Sustainable Agri-food Systems. *Potato Res.* **2021**, *64*, 681–720. [CrossRef]
3. Gikundi, E.N.; Buzera, A.K.; Orina, I.N.; Sila, D.N. Storability of Irish Potato (*Solanum tuberosum* L.) Varieties Grown in Kenya, Under Different Storage Conditions. *Potato Res.* **2023**, *66*, 137–158. [CrossRef]
4. Bedini, G.; Haff, R.P.; Benelli, A.; Bandiera, A.; Taormina, E.; Massantini, R.; Moscetti, R. Potatoes (*Solanum tuberosum* L.) grown at "Patata dell'alto Viterbese" PGI have different quality characteristics and storage responses. *Postharvest Biol. Technol.* **2024**, *214*, 112991. [CrossRef]
5. Ahmed, R.; Khanal, S.; Wang, M.; Iqbal, S.; Fan, Y.; Yi, J. Food Hydrocolloids Potato protein as an emerging high-quality: Source, extraction, purification, properties (functional, nutritional, physicochemical, and processing), applications, and challenges using potato protein. *Food Hydrocoll.* **2024**, *157*, 110415. [CrossRef]
6. Arce, A.; de Haan, S.; Juarez, H.; Burra, D.D.; Plasencia, F.; Ccanto, R.; Polreich, S.; Scurrah, M. The spatial-temporal dynamics of potato agrobiodiversity in the highlands of central Peru: A case study of smallholder management across farming landscapes. *Land* **2019**, *8*, 169. [CrossRef]
7. Chawade, A.; Van Ham, J.; Blomquist, H.; Bagge, O.; Alexandersson, E.; Ortiz, R. High-throughput field-phenotyping tools for plant breeding and precision agriculture. *Agronomy* **2019**, *9*, 258. [CrossRef]
8. Li, D.; Quan, C.; Song, Z.; Li, X.; Yu, G.; Li, C.; Muhammad, A. High-Throughput Plant Phenotyping Platform (HT3P) as a Novel Tool for Estimating Agronomic Traits From the Lab to the Field. *Front. Bioeng. Biotechnol.* **2021**, *8*, 623705. [CrossRef]
9. Yang, W.; Feng, H.; Zhang, X.; Zhang, J.; Doonan, J.H.; Batchelor, W.D.; Xiong, L.; Yan, J. Crop Phenomics and High-Throughput Phenotyping: Past Decades, Current Challenges, and Future Perspectives. *Mol. Plant* **2020**, *13*, 187–214. [CrossRef]
10. Abebe, A.M.; Kim, Y.; Kim, J.; Kim, S.L.; Baek, J. Image-Based High-Throughput Phenotyping in Horticultural Crops. *Plants* **2023**, *12*, 2061. [CrossRef]
11. Abdelhakim, L.O.A.; Pleskačová, B.; Rodriguez-Granados, N.Y.; Sasidharan, R.; Perez-Borroto, L.S.; Sonnewald, S.; Gruden, K.; Vothknecht, U.C.; Teige, M.; Panzarová, K. High Throughput Image-Based Phenotyping for Determining Morphological and Physiological Responses to Single and Combined Stresses in Potato. *J. Vis. Exp.* **2024**. [CrossRef] [PubMed]
12. Zhang, H.; Wang, L.; Jin, X.; Bian, L.; Ge, Y. High-throughput phenotyping of plant leaf morphological, physiological, and biochemical traits on multiple scales using optical sensing. *Crop J.* **2023**, *11*, 1303–1318. [CrossRef]
13. Mahlein, A.-K. Present and Future Trends in Plant Disease Detection. *Plant Dis.* **2016**, *100*, 1–11. [CrossRef]
14. Clara Gonçalves Fernandes, A.; Ribeiro Valadares, N.; Henrique Oliveira Rodrigues, C.; Aguiar Alves, R.; Lorena Melucio Guedes, L.; Luiz Mendes Athayde, A.; Azevedo, A.M. Convolutional neural networks in the qualitative improvement of sweet potato roots. *Sci. Rep.* **2023**, *13*, 1–8. [CrossRef] [PubMed]
15. Mutka, A.M.; Bart, R.S. Image-based phenotyping of plant disease symptoms. *Front. Plant Sci.* **2015**, *5*, 734. [CrossRef]
16. Di, Y.; Yang, H.; Zhang, H.; Li, F. Nitrogen management indicators for sustainable crop production in an intensive potato system under drip irrigation. *J. Environ. Manag.* **2024**, *361*, 121270. [CrossRef]
17. Kouadio, L.; El Jarroudi, M.; Belabess, Z.; Laasli, S.-E.; Roni, Z.K.; Amine, I.D.I.; Mokhtari, N.; Mokrini, F.; Junk, J.; Lahlali, R. A Review on UAV-Based Applications for Plant Disease Detection and Monitoring. *Remote Sens.* **2023**, *15*, 4273. [CrossRef]
18. Bhandari, M.; Chang, A.; Jung, J.; Ibrahim, A.M.H.; Rudd, J.C.; Baker, S.; Landivar, J.; Liu, S.; Landivar, J. Unmanned aerial system-based high-throughput phenotyping for plant breeding. *Plant Phenome J.* **2023**, *6*, e20058. [CrossRef]
19. Volpato, L.; Pinto, F.; González-Pérez, L.; Thompson, I.G.; Borém, A.; Reynolds, M.; Gérard, B.; Molero, G.; Rodrigues, F.A. High Throughput Field Phenotyping for Plant Height Using UAV-Based RGB Imagery in Wheat Breeding Lines: Feasibility and Validation. *Front. Plant Sci.* **2021**, *12*, 591587. [CrossRef]
20. Rana, S.; Gerbino, S.; Sekehravani, E.A.; Russo, M.B.; Carillo, P. Crop Growth Analysis Using Automatic Annotations and Transfer Learning in Multi-Date Aerial Images and Ortho-Mosaics. *Agronomy* **2024**, *14*, 2052. [CrossRef]
21. Ismaeal, A.S.; Farhan, M.J.; Khalaf, A.A. Wheat Crop Management and growth stage monitoring in some gypsiferous soil units using remote sensing. *Tikrit J. Agric. Sci.* **2024**, *24*, 131–160. [CrossRef]
22. Veloo, K.; Valencia-Ortiz, M.; Pumphrey, M.; Carter, A.; Pumphrey, M.; Sankaran, S. Development and Validation of a Multispectral and Thermal Sensor System for In-Field Crop Drought Stress Monitoring in Wheat. *Authorea Prepr.* **2024**. [CrossRef]
23. Samsuddin Sah, S.; Abdul Maulud, K.N.; Sharil, S.; Karim, O.A.; Pradhan, B. Monitoring of three stages of paddy growth using multispectral vegetation index derived from UAV images. *Egypt. J. Remote Sens. Space Sci.* **2023**, *26*, 989–998. [CrossRef]
24. Calcagno, F.; Romano, E.; Furnitto, N.; Jamali, A.; Failla, S. Remote Sensing Monitoring of Durum Wheat under No Tillage Practices by Means of Spectral Indices Interpretation: A Preliminary Study. *Sustainability* **2022**, *14*, 15012. [CrossRef]
25. Liang, Y.; Li, H.; Wu, H.; Zhao, Y.; Liu, Z.; Liu, D.; Liu, Z.; Fan, G.; Pan, Z.; Shen, Z.; et al. A rotated rice spike detection model and a crop yield estimation application based on UAV images. *Comput. Electron. Agric.* **2024**, *224*, 109188. [CrossRef]
26. Tripathi, A.; Tiwari, R.K.; Tiwari, S.P. A deep learning multi-layer perceptron and remote sensing approach for soil health based crop yield estimation. *Int. J. Appl. Earth Obs. Geoinf.* **2022**, *113*, 102959. [CrossRef]
27. Liu, J.; Xu, X.; Liu, Y.; Rao, Z.; Smith, M.L.; Jin, L.; Li, B. Quantitative potato tuber phenotyping by 3D imaging. *Biosyst. Eng.* **2021**, *210*, 48–59. [CrossRef]

28. Su, Q.; Kondo, N.; Li, M.; Sun, H.; Al Riza, D.F.; Habaragamuwa, H. Potato quality grading based on machine vision and 3D shape analysis. *Comput. Electron. Agric.* **2018**, *152*, 261–268. [CrossRef]
29. Golmohammadi, A.; Afkari-Sayyah, A.H. Long-Term Storage Effects on the Physical Properties of the Potato. *Int. J. Food Prop.* **2013**, *16*, 104–113. [CrossRef]
30. Zhuo, W.; Fang, S.; Wu, D.; Wang, L.; Li, M.; Zhang, J.; Gao, X. Integrating remotely sensed water stress factor with a crop growth model for winter wheat yield estimation in the North China Plain during. *Crop J.* **2022**, *10*, 1470–1482. [CrossRef]
31. Marshall, M.; Belgiu, M.; Boschetti, M.; Pepe, M.; Stein, A.; Nelson, A. ISPRS Journal of Photogrammetry and Remote Sensing Field-level crop yield estimation with PRISMA and Sentinel-2. *ISPRS J. Photogramm. Remote Sens.* **2022**, *187*, 191–210. [CrossRef]
32. Elshikha, D.E.M.; Hunsaker, D.J.; Waller, P.M.; Thorp, K.R.; Dierig, D.; Wang, G.; Cruz, V.M.V.; Katterman, M.E.; Bronson, K.F.; Wall, G.W.; et al. Estimation of direct-seeded guayule cover, crop coefficient, and yield using UAS-based multispectral and RGB data. *Agric. Water Manag.* **2022**, *265*, 107540. [CrossRef]
33. De la Casa, A.; Ovando, G.; Bressanini, L.; Martínez, J.; Díaz, G.; Miranda, C. Soybean crop coverage estimation from NDVI images with different spatial resolution to evaluate yield variability in a plot. *ISPRS J. Photogramm. Remote Sens.* **2018**, *146*, 531–547. [CrossRef]
34. Wei, Z.; Fang, W. Smart Agricultural Technology UV-NDVI for real-time crop health monitoring in vertical farms. *Smart Agric. Technol.* **2024**, *8*, 100462. [CrossRef]
35. Roznik, M.; Boyd, M.; Porth, L. Improving crop yield estimation by applying higher resolution satellite NDVI imagery and high-resolution cropland masks. *Remote Sens. Appl.* **2022**, *25*, 100693. [CrossRef]
36. Leroux, L.; Castets, M.; Baron, C.; Escorihuela, M.; Bégué, A.; Lo, D. Maize yield estimation in West Africa from crop process-induced combinations of multi-domain remote sensing indices. *Eur. J. Agron.* **2019**, *108*, 11–26. [CrossRef]
37. Chen, Y.; Tao, F. Improving the practicability of remote sensing data-assimilation-based crop yield estimations over a large area using a spatial assimilation algorithm and ensemble assimilation strategies. *Agric. For. Meteorol.* **2020**, *291*, 108082. [CrossRef]
38. Sumesh, K.C.; Ninsawat, S.; Som-ard, J. Integration of RGB-based vegetation index, crop surface model and object-based image analysis approach for sugarcane yield estimation using unmanned aerial vehicle. *Comput. Electron. Agric.* **2021**, *180*, 105903. [CrossRef]
39. Martins, I.; Junior, F.; Vianna, S. Assimilating leaf area index data into a sugarcane process-based crop model for improving yield estimation. *Eur. J. Agron.* **2022**, *136*, 126501. [CrossRef]
40. Miller, J.O.; Mondal, P.; Sarupria, M. Sensor-based measurements of NDVI in small grain and corn fi elds by tractor, drone, and satellite platforms. *Crop Environ.* **2024**, *3*, 33–42. [CrossRef]
41. Parida, P.K.; Somasundaram, E.; Krishnan, R.; Radhamani, S.; Sivakumar, U.; Parameswari, E.; Raja, R.; Shri Rangasami, S.R.; Sangeetha, S.P.; Gangai Selvi, R. Unmanned Aerial Vehicle-Measured Multispectral Vegetation Indices for Predicting LAI, SPAD Chlorophyll, and Yield of Maize. *Agriculture* **2024**, *14*, 1110. [CrossRef]
42. Han, Y. Application of Unmanned Aerial Vehicle Remote Sensing for Agricultural Monitoring. *E3S Web Conf.* **2024**, *553*, 02022. [CrossRef]
43. Sankaran, S.; Quirós, J.J.; Miklas, P.N. Unmanned aerial system and satellite-based high resolution imagery for high-throughput phenotyping in dry bean. *Comput. Electron. Agric.* **2019**, *165*, 104965. [CrossRef]
44. Ivushkin, K.; Bartholomeus, H.; Bregt, A.K.; Pulatov, A.; Franceschini, M.H.; Kramer, H.; van Loo, E.N.; Roman, V.J.; Finkers, R. UAV based soil salinity assessment of cropland. *Geoderma* **2019**, *338*, 502–512. [CrossRef]
45. ten Harkel, J.; Bartholomeus, H.; Kooistra, L. Biomass and crop height estimation of different crops using UAV-based LiDAR. *Remote Sens.* **2020**, *12*, 17. [CrossRef]
46. Ibiev, G.Z.; Savoskina, O.A.; Chebanenko, S.I.; Beloshapkina, O.O.; Zavertkin, I.A. Unmanned Aerial Vehicles (UAVs)—One of the Digitalization and Effective Development Segments of Agricultural Production in Modern Conditions. *AIP Conf. Proc.* **2022**, *2661*, 070007. [CrossRef]
47. Yang, Y.; Su, X. Spatial correlation network structure of carbon emission reduction capacity on urban agglomerations and its driving factors: A perspective of Sustainable Development Goals. *Sustain. Cities Soc.* **2024**, *113*, 105646. [CrossRef]
48. Garcia, C.; López-Jiménez, P.A.; Pérez-Sánchez, M.; Sanchis, R. Methodology for assessing progress in sustainable development goals indicators in urban water systems. How far are we from the 2030 targets? *Sustain. Cities Soc.* **2024**, *112*, 105616. [CrossRef]
49. Senamhi. Climas del Perú Mapa de Cllasificación Climática Nacional. Volume 53. 2020. Available online: https://www.senamhi.gob.pe/load/file/01404SENA-4.pdf (accessed on 22 September 2024).
50. Ccopi-Trucios, D.; Barzola-Rojas, B.; Ruiz-Soto, S.; Gabriel-Campos, E.; Ortega-Quispe, K.; Cordova-Buiza, F. River Flood Risk Assessment in Communities of the Peruvian Andes: A Semiquantitative Application for Disaster Prevention. *Sustainability* **2023**, *15*, 13768. [CrossRef]
51. Ortega Quispe, K.A.; Valerio Deudor, L.L. Captación y almacenamiento pluvial como modelo histórico para conservación del agua en los Andes peruanos. *Desafios* **2023**, *14*, e385. [CrossRef]
52. Hijmans, J. Package "terra" Spatial Data Analysis 2024. Available online: https://cran.r-project.org/web/packages/terra/index.html (accessed on 22 September 2024).
53. Gitelson, A.A.; Kaufman, Y.J.; Merzlyak, M.N. Use of a green channel in remote sensing of global vegetation from EOS-MODIS. *Remote Sens. Environ.* **1996**, *58*, 289–298. [CrossRef]
54. Jordan, C.F. Derivation of Leaf-Area Index from Quality of Light on the Forest Floor. *Ecology* **1969**, *50*, 663–666. [CrossRef]

55. Wu, C.; Niu, Z.; Gao, S. The potential of the satellite derived green chlorophyll index for estimating midday light use efficiency in maize, coniferous forest and grassland. *Ecol. Indic.* **2012**, *14*, 66–73. [CrossRef]
56. Gitelson, A.A.; Gritz, Y.; Merzlyak, M.N. Relationships between leaf chlorophyll content and spectral reflectance and algorithms for non-destructive chlorophyll assessment in higher plant leaves. *J. Plant Physiol.* **2003**, *160*, 271–282. [CrossRef] [PubMed]
57. Schleicher, T.D.; Bausch, W.C.; Delgado, J.A.; Ayers, P.D. Evaluation and Refinement of the Nitrogen. Reflectance Index. (NRI) for Site-Specific Fertilizer Management. In *2001 ASAE Annual Meeting*; American Society of Agricultural and Biological Engineers: St. Joseph, MI, USA, 1998; p. 1. [CrossRef]
58. Pereira, F.S.; de Lima, J.; Freitas, R.; Dos Reis, A.; Amaral, L.; Figueiredo, G.; Lamparelli, R.; Magalhães, P. Nitrogen variability assessment of pasture fields under an integrated crop-livestock system using UAV, PlanetScope, and Sentinel-2 data. *Comput. Electron. Agric.* **2022**, *193*, 106645. [CrossRef]
59. Yang, C.; Everitt, J.H.; Bradford, J.M.; Murden, D. Airborne hyperspectral imagery and yield monitor data for mapping cotton yield variability. *Precis. Agric.* **2004**, *5*, 445–461. [CrossRef]
60. Meyer, G.E.; Neto, J.C. Verification of color vegetation indices for automated crop imaging applications. *Comput. Electron. Agric.* **2008**, *63*, 282–293. [CrossRef]
61. Strong, C.J.; Burnside, N.G.; Llewellyn, D. The potential of small-Unmanned Aircraft Systems for the rapid detection of threatened unimproved grassland communities using an Enhanced Normalized Difference Vegetation Index. *PLoS ONE* **2017**, *12*, e0186193. [CrossRef]
62. Mokarram, M.; Hojjati, M.; Roshan, G.; Negahban, S. Modeling the behavior of Vegetation Indices in the salt dome of Korsia in North-East of Darab, Fars, Iran. *Model. Earth Syst. Environ.* **2015**, *1*, 1–9. [CrossRef]
63. A Method of Assigning Numerical and Percentage Values to the Degree of Roundness of Sand Grains on JSTOR n.d. Available online: https://www.jstor.org/stable/1298056 (accessed on 18 September 2024).
64. Aswin Kumer, S.V.; Kanakaraja, P.; Areez, S.; Patnaik, Y.; Tarun Kumar, P. An implementation of virtual white board using open CV for virtual classes. *Mater. Today Proc.* **2021**, *46*, 4031–4034. [CrossRef]
65. Harris, C.R.; Millman, K.J.; van der Walt, S.J.; Gommers, R.; Virtanen, P.; Cournapeau, D.; Wieser, E.; Taylor, J.; Berg, S.; Smith, N.J.; et al. Array programming with NumPy. *Nature* **2020**, *585*, 357–362. [CrossRef] [PubMed]
66. Hunter, J.D. Matplotlib: A 2D graphics environment. *Comput. Sci. Eng.* **2007**, *9*, 90–95. [CrossRef]
67. Neilson, J.A.D.; Smith, A.M.; Mesina, L.; Vivian, R.; Smienk, S.; De Koyer, D. Potato tuber shape phenotyping using RGB imaging. *Agronomy* **2021**, *11*, 1781. [CrossRef]
68. Ruiz de Arcaute, R.; Carrasco, A.; Ortega, F.; Rodriguez-Quijano, M.; Carrillo, J.M. Evaluation of Genetic Resources in a Potato Breeding Program for Chip Quality. *Agronomy* **2022**, *12*, 1142. [CrossRef]
69. Tedesco, D.; de Oliveira, M.F.; dos Santos, A.F.; Costa Silva, E.H.; de Souza Rolim, G.; da Silva, R.P. Use of remote sensing to characterize the phenological development and to predict sweet potato yield in two growing seasons. *Eur. J. Agron.* **2021**, *129*, 126337. [CrossRef]
70. Reategui, K.; Aguirre, N.; Oliva, R.; Aguirre, E. Phenology and yield of four potato varieties in the Peruvian Altiplano. *Sci. Agropecu.* **2019**, *10*, 265–274. [CrossRef]
71. Li, L.; Zhang, Q.; Huang, D. A review of imaging techniques for plant phenotyping. *Sensors* **2014**, *14*, 20078–20111. [CrossRef]
72. Bashir, R.N.; Mzoughi, O.; Shahid, M.A.; Alturki, N.; Saidani, O. Principal Component Analysis (PCA) and feature importance-based dimension reduction for Reference Evapotranspiration (ET0) predictions of Taif, Saudi Arabia. *Comput. Electron. Agric.* **2024**, *222*, 109036. [CrossRef]
73. Chaukhande, P.; Luthra, S.K.; Patel, R.N.; Padhi, S.R.; Mankar, P.; Mangal, M.; Ranjan, J.K.; Solanke, A.U.; Mishra, G.P.; Mishra, D.C.; et al. Development and Validation of Near-Infrared Reflectance Spectroscopy Prediction Modeling for the Rapid Estimation of Biochemical Traits in Potato. *Foods* **2024**, *13*, 1655. [CrossRef]
74. Buckner, C.A.; Lafrenie, R.M.; Dénommée, J.A.; Caswell, J.M.; Want, D.A.; Gan, G.G.; Leong, Y.C.; Bee, P.C.; Chin, E.; Teh, A.K.H.; et al. We are IntechOpen, the world' s leading publisher of Open Access books Built by scientists, for scientists TOP 1%. *Intech* **2016**, *11*, 13.
75. Kok, Z.H.; Mohamed Shariff, A.R.; Alfatni, M.S.M.; Khairunniza-Bejo, S. Support Vector Machine in Precision Agriculture: A review. *Comput. Electron. Agric.* **2021**, *191*, 106546. [CrossRef]
76. Pizarro, S.; Pricope, N.G.; Figueroa, D.; Carbajal, C.; Quispe, M.; Vera, J.; Alejandro, L.; Achallma, L.; Gonzalez, I.; Salazar, W.; et al. Implementing Cloud Computing for the Digital Mapping of Agricultural Soil Properties from High Resolution UAV Multispectral Imagery. *Remote Sens.* **2023**, *15*, 3203. [CrossRef]
77. Kalecinski, N.I.; Skakun, S.; Torbick, N.; Huang, X.; Roger, J.; Vermote, E. Crop yield estimation at different growing stages using a synergy of SAR and optical remote sensing data. *Sci. Remote Sens.* **2024**, *10*, 100153. [CrossRef]
78. Wang, Q.; Zou, X.; Chen, Y.; Zhu, Z.; Yan, C.; Shan, P.; Wang, S.; Fu, Y. XGBoost algorithm assisted multi-component quantitative analysis with Raman spectroscopy. *Spectrochim. Acta A Mol. Biomol. Spectrosc.* **2024**, *323*, 124917. [CrossRef]
79. Corte, A.P.D.; Rex, F.E.; de Almeida, D.R.A.; Sanquetta, C.R.; Silva, C.A.; Moura, M.M.; Wilkinson, B.; Zambrano, A.M.A.; da Cunha Neto, E.M.; Veras, H.F.P.; et al. Measuring individual tree diameter and height using gatoreye high-density UAV-lidar in an integrated crop-livestock-forest system. *Remote Sens.* **2020**, *12*, 863. [CrossRef]
80. Abdikan, S.; Sekertekin, A.; Narin, O.G.; Delen, A.; Balik Sanli, F. A comparative analysis of SLR, MLR, ANN, XGBoost and CNN for crop height estimation of sunflower using Sentinel-1 and Sentinel-2. *Adv. Space Res.* **2023**, *71*, 3045–3059. [CrossRef]

81. Anandan, B.; Manikandan, M. Machine learning approach with various regression models for predicting the ultimate tensile strength of the friction stir welded AA 2050-T8 joints by the K-Fold cross-validation method. *Mater. Today Commun.* **2023**, *34*, 105286. [CrossRef]
82. Ait tchakoucht, T.; Elkari, B.; Chaibi, Y.; Kousksou, T. Random forest with feature selection and K-fold cross validation for predicting the electrical and thermal efficiencies of air based photovoltaic-thermal systems. *Energy Rep.* **2024**, *12*, 988–999. [CrossRef]
83. Berrar, D. Cross-Validation. Reference Module in Life Sciences. 2024. Available online: https://www.sciencedirect.com/science/article/abs/pii/B9780323955027000324?via=ihub (accessed on 22 September 2024).
84. Kuhn, M.; Johnson, K. Applied Predictive Modeling n.d. Available online: https://vuquangnguyen2016.wordpress.com/wp-content/uploads/2018/03/applied-predictive-modeling-max-kuhn-kjell-johnson_1518.pdf (accessed on 22 September 2024).
85. Trentin, C.; Ampatzidis, Y.; Lacerda, C.; Shiratsuchi, L. Tree crop yield estimation and prediction using remote sensing and machine learning: A systematic review. *Smart Agric. Technol.* **2024**, *9*, 100556. [CrossRef]
86. Nejad, S.M.M.; Abbasi-Moghadam, D.; Sharifi, A.; Tariq, A. Capsular attention Conv-LSTM network (CACN): A deep learning structure for crop yield estimation based on multispectral imagery. *Eur. J. Agron.* **2024**, *161*, 127369. [CrossRef]
87. Willmott, C.J.; Matsuura, K. Advantages of the mean absolute error (MAE) over the root mean square error (RMSE) in assessing average model performance. *Clim. Res.* **2005**, *30*, 79–82. [CrossRef]
88. Chai, T.; Draxler, R.R. Root mean square error (RMSE) or mean absolute error (MAE)? -Arguments against avoiding RMSE in the literature. *Geosci. Model. Dev.* **2014**, *7*, 1247–1250. [CrossRef]
89. Guo, Y.; Zhang, L.; Li, Z.; He, Y.; Lv, C.; Chen, Y.; Lv, H.; Du, Z. Online Detection of Dry Matter in Potatoes Based on Visible Near-Infrared Transmission Spectroscopy Combined with 1D-CNN. *Agriculture* **2024**, *14*, 787. [CrossRef]
90. Nolasco, M. Maestría en Aplicaciones Espaciales de Alerta y Respuesta MEW 9, Seminario Autor: Ing. Agr. Miguel Nolasco. 2020. Available online: https://www.researchgate.net/publication/345034023_ANALISIS_DE_BORDE_ROJO_RED_EDGE_EN_LA_DETERMINACION_DE_INDICES_DE_VEGETACION?channel=doi&linkId=5f9c7b9492851c14bcf638ef&showFulltext=true (accessed on 22 September 2024).
91. Taşan, S.; Cemek, B.; Taşan, M.; Cantürk, A. Estimation of eggplant yield with machine learning methods using spectral vegetation indices. *Comput. Electron. Agric.* **2022**, *202*, 107367. [CrossRef]
92. Adugna, T.; Xu, W.; Fan, J. Comparison of Random Forest and Support Vector Machine Classifiers for Regional Land Cover Mapping Using Coarse Resolution FY-3C Images. *Remote Sens.* **2022**, *14*, 574. [CrossRef]
93. Fan, Y.; Liu, Y.; Yue, J.; Jin, X.; Chen, R.; Bian, M.; Ma, Y.; Yang, G.; Feng, H. Estimation of potato yield using a semi-mechanistic model developed by proximal remote sensing and environmental variables. *Comput. Electron. Agric.* **2024**, *223*, 109117. [CrossRef]
94. Šťastná, M.; Toman, F.; Dufková, J. Usage of SUBSTOR model in potato yield prediction. *Agric. Water Manag.* **2010**, *97*, 286–290. [CrossRef]
95. Priyatikanto, R.; Lu, Y.; Dash, J.; Sheffield, J. Improving generalisability and transferability of machine-learning-based maize yield prediction model through domain adaptation. *Agric. For. Meteorol.* **2023**, *341*, 109652. [CrossRef]
96. Hoppe, H.; Dietrich, P.; Marzahn, P.; Weiß, T.; Nitzsche, C.; von Lukas, U.F.; Wengerek, T.; Borg, E. Transferability of Machine Learning Models for Crop Classification in Remote Sensing Imagery Using a New Test Methodology: A Study on Phenological, Temporal, and Spatial Influences. *Remote Sens.* **2024**, *16*, 1493. [CrossRef]
97. Pokhariyal, S.; Patel, N.R.; Govind, A. Machine Learning-Driven Remote Sensing Applications for Agriculture in India—A Systematic Review. *Agronomy* **2023**, *13*, 2302. [CrossRef]
98. Dhillon, M.S.; Dahms, T.; Kuebert-Flock, C.; Rummler, T.; Arnault, J.; Steffan-Dewenter, I.; Ullmann, T. Integrating random forest and crop modeling improves the crop yield prediction of winter wheat and oil seed rape. *Front. Remote Sens.* **2022**, *3*, 1010978. [CrossRef]
99. Lischeid, G.; Webber, H.; Sommer, M.; Nendel, C.; Ewert, F. Machine learning in crop yield modelling: A powerful tool, but no surrogate for science. *Agric. For. Meteorol.* **2022**, *312*, 108698. [CrossRef]
100. Qadeer, A.; Shakir, M.; Wang, L.; Talha, S.M. Evaluating machine learning approaches for aboveground biomass prediction in fragmented high-elevated forests using multi-sensor satellite data. *Remote Sens. Appl.* **2024**, *36*, 101291. [CrossRef]